Possible experimentally observable effects of vertex corrections in superconductors

P. Miller and J. K. Freericks
Department of Physics, Georgetown University, Washington, D.C. 20057-0995

E. J. Nicol
Department of Physics, University of Guelph, Guelph, Ontario, Canada

(Received 20 May 1998)

We calculate the effects of vertex corrections, of nonconstant density of states and of a (self-consistently determined) phonon self-energy for the Holstein model on a three-dimensional cubic lattice. We replace vertex corrections with a Coulomb pseudopotential μ_C^* adjusted to give the same T_c, and repeat the calculations, to see which effects are a distinct feature of vertex corrections. This allows us to determine directly observable effects of vertex corrections on a variety of thermodynamic properties of superconductors. To this end, we employ conserving approximations (in the local approximation) to calculate the superconducting critical temperatures, isotope coefficients, superconducting gaps, free-energy differences, and thermodynamic critical fields for a range of parameters. We find that the dressed value of λ is significantly larger than the bare value. While vertex corrections can cause significant changes in all the above quantities (even when the bare electron-phonon coupling is small), the changes can usually be well modeled by an appropriate Coulomb pseudopotential. The isotope coefficient proves to be the quantity that most clearly shows effects of vertex corrections that can not be mimicked by a μ_C^*. [S0163-1829(98)05245-X]

I. INTRODUCTION

The theory of conventional, low-temperature superconductors has been well understood for decades, within BCS theory,[1] and many material properties of superconductors have been accurately described within the more appropriate Migdal-Eliashberg formalism,[2,3] which includes the retardation effects of the electron-phonon interaction in a realistic manner. The success of the formalism arises from Migdal's theorem,[2] which says that vertex corrections can be neglected when the ratio of the phonon energy scale to the electron energy scale is small (such as the value of 10^{-4} typical of conventional low-temperature superconductors). The physical reason being that the ion movement is typically too slow to respond to anything but the mean-field potential produced by the fast-moving electrons.

In recent years there has been investigation of superconducting materials[4–10] such as $Ba_{1-x}K_xBiO_3$, K_3C_{60}, and the $A15$'s, whose phonon energy scale is a larger fraction of their electron energy scale. For such materials, the standard Migdal-Eliashberg theory may no longer be valid, either because second-order processes in the electron-phonon coupling (so-called vertex corrections) can not be neglected,[11–15] or because structure in the electronic density of states and finite-bandwidth effects become significant.[16] Our aim is to identify those experiments which can clearly indicate where vertex corrections, or structure in the electronic density of states, are observable in real materials. In particular, we wish to uncover those effects which can not be mimicked by a Coulomb pseudopotential μ_C^* as this would render them unobservable in practice, because a μ_C^* is typically fitted to the experimental data.

The most compelling evidence for the effect of vertex corrections would come from a tunneling conductance measurement that provided data for the tunneling conductance out to an energy at least twice that of the maximal phonon frequency of the bulk material. Then a tunneling inversion could be performed using only the experimental data out to an energy of the maximal bulk phonon energy, and the results for Migdal-Eliashberg theory would be compared to the vertex-corrected theory for the experimental data that was measured in the multiphonon region, at voltages above the maximal bulk phonon energy of the material. Unfortunately, such an analysis has only been performed for lead[12] and in that case, the experimental data was not accurate enough in the multiphonon region to be able to see if effects of vertex corrections were observable. Similarly, high energy data from optical conductivity experiments would indicate whether or not vertex corrections are important, but there again, the accuracy of the data might preclude seeing effects of vertex corrections.

In order to determine what effects are unmistakenly due to vertex corrections, we fit a Coulomb pseudopotential μ_C^* to a Migdal-Eliashberg theory so that the superconducting transition temperature T_c is the same for the vertex-corrected theory (with no μ_C^*) and the conventional Migdal-Eliashberg theory (with a μ_C^* but no vertex corrections). In the case of dressed phonons, we adjust both the electron-phonon interaction energy and μ_C^*, in order to fit the same values of λ and T_c as the results with vertex corrections. This procedure is exactly the procedure carried out in analyzing experimental data within the conventional theory. We carry out this ''experimental analysis'' on a model system where we know that vertex corrections have a large effect, in order to see the extent to which the conventional analysis masks their observation. Hence we look for differences in thermodynamic quantities between these results and those with vertex corrections. Any quantities which are significantly different

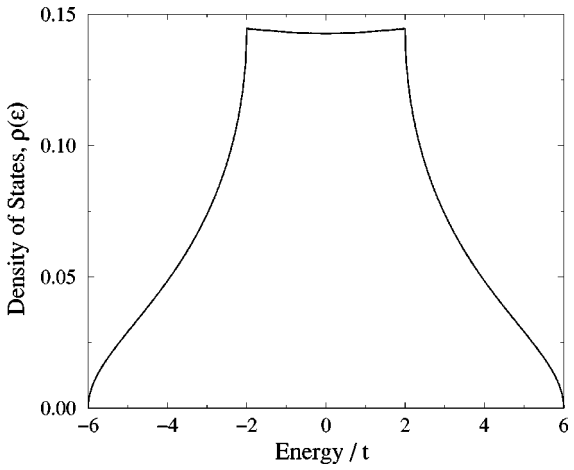

FIG. 1. The single-spin density of states for noninteracting electrons on a 3D cubic tight-binding lattice. Note the nature of the van Hove singularities, which lead to an abrupt fall in the density of states. They occur at electron fillings of $n \approx 0.45$ and $n \approx 1.55$. The approximate form used in the calculations is also plotted, and is indistinguishable by eye from the exact curve.

when calculated with a fitted μ_C^* instead of vertex corrections pin-point the experiments that can give the best indication that a material needs to have vertex corrections included in its description.

Since this is the initial attempt at solving such a problem, we study a simple model system, which has a nonconstant electronic density of states (Fig. 1), using both Migdal-Eliashberg formalism, and going beyond it, to include vertex corrections. The vertex corrections are second-order diagrams where a pair of phonon lines cross, as shown in the self-energies of Fig. 2(b). In both cases, the phonon propagators can be dressed (i.e., with a phonon self-energy included) or bare, as shown in Fig. 2. We find that dressing the phonons leads to a strong enhancement of the effective interaction strength, exemplified by a large renormalization in the value of the electron-phonon coupling parameter λ.

The specific model we study is the Holstein Hamiltonian[17] on a three-dimensional (3D) cubic lattice. The Hamiltonian consists of conduction electrons that hop from site to site, coupled to harmonic, localized (Einstein) phonons:

$$\hat{H} - \mu \hat{N} = \sum_{i,j,\sigma} t_{ij} \hat{c}_{i\sigma}^{\dagger} \hat{c}_{j\sigma} + \frac{1}{2} M \Omega^2 \sum_i \hat{x}_i^2 + \frac{1}{2M} \sum_i \hat{p}_i^2 + \sum_i (g \hat{x}_i - \mu) \hat{n}_i , \qquad (1)$$

where $\hat{c}_{i\sigma}^{\dagger}$ and $\hat{c}_{i\sigma}$ are fermionic operators which create and destroy, respectively, an electron of spin σ in a single Wannier (tight-binding) state on the lattice site i, whose total electron occupancy is given by $n_i = \hat{c}_{i\uparrow}^{\dagger} \hat{c}_{i\uparrow} + \hat{c}_{i\downarrow}^{\dagger} \hat{c}_{i\downarrow}$. The electron hopping is between nearest neighbors only, such that $t_{ij} = -t$ if i,j are neighboring sites, with t the overlap integral, and $t_{ij} = 0$ otherwise. The phonons, of mass M with displacement x_i and momentum p_i are characterized by their

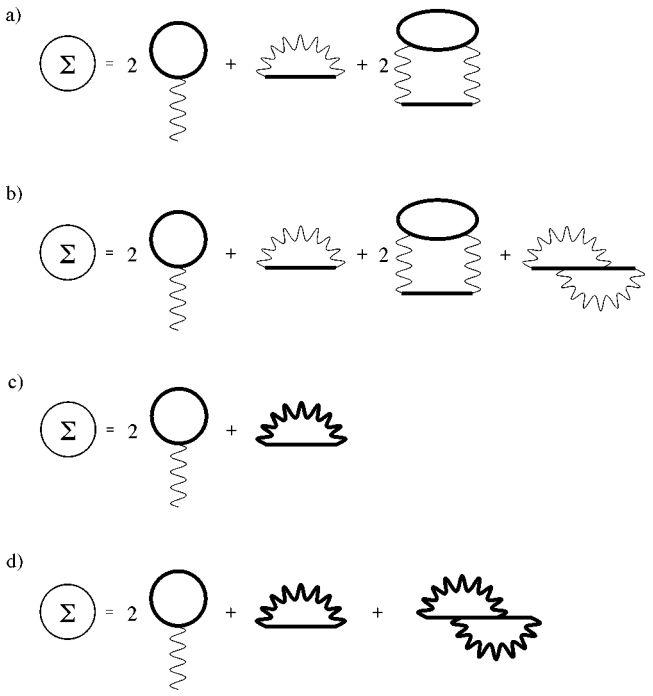

FIG. 2. Different forms for the electron self-energy. All diagrams include the same initial Hartree term, followed by the specific Fock contribution and any other required diagrams. All electronic Green's functions are dressed, but phonon lines can be undressed (thin) or dressed (thick) as in Fig. 3(b). For bare phonons, (a) is with no vertex corrections, while (b) includes the vertex-corrected diagram. When the phonons are dressed, (c) is without vertex corrections, while (d) includes them. A factor of 2 appears in front of each electron loop term, to indicate a sum over spins.

frequency Ω. The strength of the bare electron-phonon coupling can be measured by the bipolaron binding energy U, where

$$U = -\frac{g^2}{M\Omega^2}. \qquad (2)$$

The chemical potential is μ, and is always calculated self-consistently for a given average number of electrons per site n $(0 \leqslant n \leqslant 2)$. Particle-hole symmetry occurs at half filling, where $n = 1$ and $\mu = U$. We concentrate our work on superconductivity and ignore any possible charge-density wave order that may occur near half filling.

We carry out weak-coupling expansions within the conserving approximations of Baym and Kadanoff.[18–21] The electron self-energy Σ is given as a functional derivative of the free-energy functional Φ with respect to the electron Green's function G. When dressing the phonons, we maintain a conserving approximation by careful choice of the phonon self-energy. In this case, there must be a free-energy functional Φ whose *partial* derivative with respect to the electron Green's function yields the electron self-energy *and* whose *partial* derivative with respect to the phonon Green's function D yields the phonon self-energy. In such cases there always exists a related free-energy functional Φ', which is the skeleton-diagram expansion whose *full* functional derivative with respect to the electron Green's function yields the electron self-energy. In all cases, the irreducible vertex func-

tion is given by the *full* functional derivative of the electron self-energy with respect to the electron Green's function, i.e., $T\Gamma_{n,m}=d\Sigma(i\omega_n)/dG(i\omega_m)$.

We employ the local approximation in our calculations, which means we neglect the momentum dependence in the self-energy and irreducible vertex functions. The local problem gives an exact solution in the infinite-dimensional limit,[11,22] but in this case it is an approximation, which, as used in Migdal-Eliashberg theory, is expected to give good quantitative results, though of course it means we can only study *s*-wave pairing.

We use the formalism, described in detail in the next section, to calculate the critical temperature T_c and the isotope coefficient α by looking at the instability of the normal state. Also, within the superconducting state, we calculate the superconducting gap Δ and the thermodynamic critical field H_c from the free-energy difference F_S-F_N. The conserving nature of each approximation is evidenced from the fact that the T_c determined by extrapolating the ordered-phase calculations to zero order parameter agrees withe the T_c found from the Owen-Scalapino method[23] in the normal state. We point out in particular those results which deviate from Migdal-Eliashberg theory, and arise from vertex corrections or a nonconstant density of states. By including a Coulomb pseudopotential, which causes the same change in T_c as vertex corrections, we are able to demonstrate what experiments can be used to differentiate between vertex corrections and a Coulomb pseudopotential.

Section II contains the formalism, describing the particular approximations we use, and explaining how our calculations are carried out. Section III presents our computational results, including a number of graphs depicting the various quantities that can be determined experimentally for real systems. We make our conclusions in Sec. IV, which is followed by an Appendix which gives the detailed formula withheld from Sec. II.

II. FORMALISM

In our calculations, we use four different types of conserving approximations, which will be expounded below. Four different approximations are necessary, in order to reveal how dressing the ''bare'' phonons affects solutions of the model, as well as to demonstrate the effects of vertex corrections. Each approximation includes a specific self-energy, and hence a specific vertex function, as shown in Figs. 2–5. In short, these can be described as (a) Migdal-Eliashberg approximation with a truncated dressing of phonons, (b) second-order perturbation theory, which contains vertex corrections and a truncated dressing of phonons, (c) Migdal-Eliashberg theory with dressed phonons (also known as the shielded potential approximation[19]), and (d) vertex-corrected theory with dressed phonons.

The calculations are carried out on the imaginary axis,[22] with the Green's functions and self-energies defined at Matsubara frequencies $i\omega_n=(2n+1)\pi iT$, where T is the temperature. The self-energies are calculated from the derivative of an appropriate free-energy functional Φ as

$$\Sigma(i\omega_n)=\frac{1}{T}\frac{\delta\Phi}{\delta G^{\uparrow\uparrow}(i\omega_n)}, \quad \phi(i\omega_n)=\frac{1}{T}\frac{\delta\Phi}{\delta F^{*}(i\omega_n)},$$

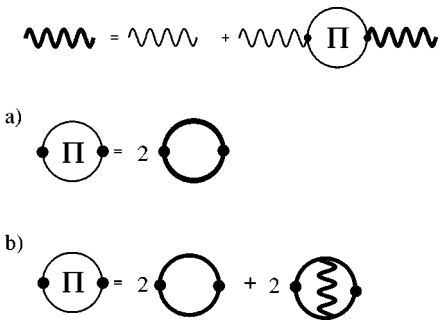

FIG. 3. Dyson's equation for the phonon propagators. Thin lines indicate bare Green's functions while thick lines indicate dressed ones. (a) is the phonon self-energy without vertex corrections, (b) is with vertex corrections. The factors of 2 come from a sum over electron spins.

while the irreducible vertex function for superconductivity is given by

$$T\Gamma_{n,m}=\frac{\delta\phi(i\omega_n)}{\delta F(i\omega_m)}.$$

Figure 4 shows the Feynman diagrams which correspond to the appropriate free-energy functional Φ for each of the four calculations, while we defer the specific formulas to the ap-

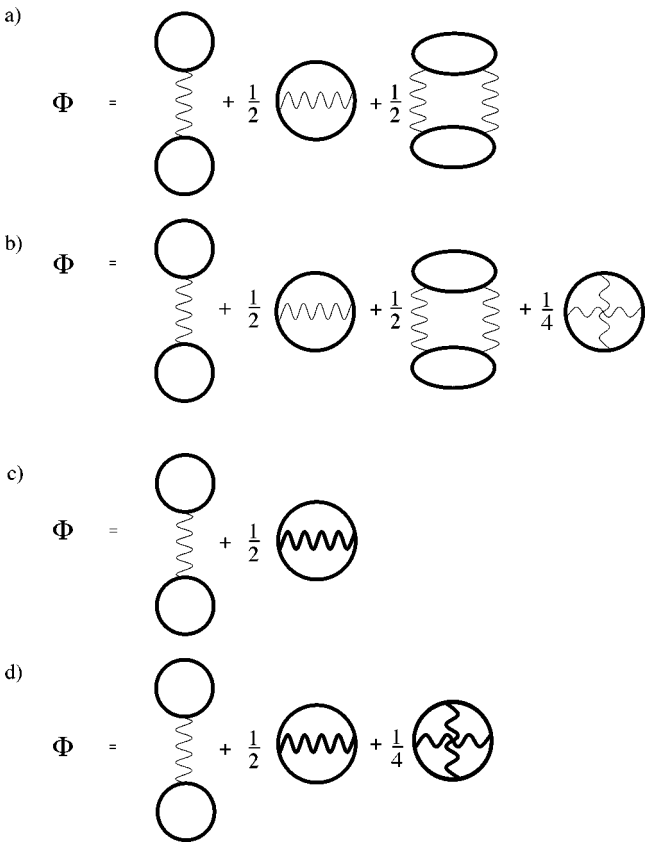

FIG. 4. Free-energy functional Φ for the conserving approximations. Equations (a) and (b) are with bare phonon propagators, while (c) and (d) have dressed phonons. The first term on the right in each equation is the Hartree term, which does not change and which is not included in Φ'. (Its phonon line is always undressed, to avoid double counting). The extra, final diagram in (b) and (d) is the vertex-correction term.

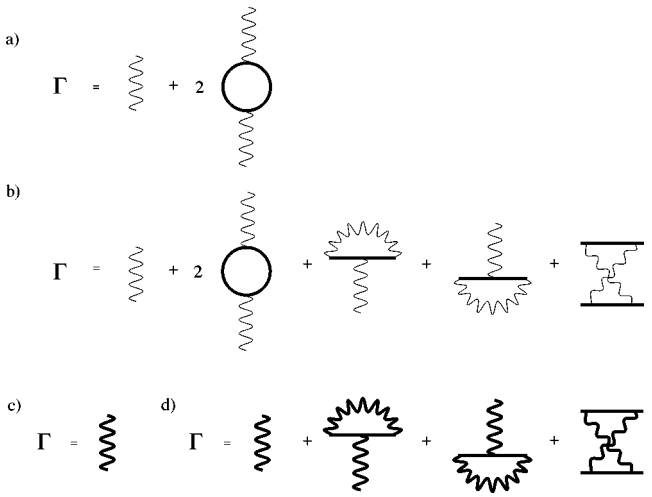

FIG. 5. The irreducible vertex-function diagrams, for superconductivity. (a) is with no vertex corrections, while (b) includes the three vertex-corrected diagrams. When the phonons are dressed, (c) is without vertex corrections, while (d) includes them.

pendix. The functional Φ' whose *full* derivative leads to the electronic self-energy, is equal to Φ when the phonons are ''bare,'' but consists of an infinite number of skeleton diagrams when the phonons are dressed. The precise relationship between Φ' and Φ is given in Eq. (A18).

When calculating properties for the superconducting state, we must use the Nambu formalism,[24] where the electron Green's function and self-energy are represented by a 2×2 matrix

$$\underline{\underline{G}}(i\omega_n)\equiv\begin{pmatrix} G^{\uparrow\uparrow}(i\omega_n) & F(i\omega_n) \\ F^*(i\omega_n) & -G^{\downarrow\downarrow}(-i\omega_n)\end{pmatrix}$$
$$=\int \rho^{(0)}(\epsilon)d\epsilon[i\omega_n\underline{\underline{\tau}}_3-\epsilon+\mu-\underline{\underline{\Sigma}}(i\omega_n)]^{-1}, \quad (3)$$

where $\rho^{(0)}(\epsilon)$ is the approximate form for the noninteracting electron density of states on a 3D cubic lattice as shown in Fig. 1, given by Uhrig,[25] and

$$\underline{\underline{\Sigma}}(i\omega_n)\equiv\begin{pmatrix} \Sigma(i\omega_n) & \phi(i\omega_n) \\ \phi^*(i\omega_n) & \Sigma^*(i\omega_n)\end{pmatrix},$$
$$\underline{\underline{\tau}}_3=\begin{pmatrix} 1 & 0 \\ 0 & -1\end{pmatrix}. \quad (4)$$

Here, the diagonal and off-diagonal Green's functions are defined respectively as

$$G^{\sigma\sigma}(i\omega_n)=-\frac{1}{N}\sum_j \int_0^\beta d\tau \exp(i\omega_n\tau)\langle \mathrm{T}_\tau \hat{c}_{j\sigma}(\tau)\hat{c}^\dagger_{j\sigma}(0)\rangle, \quad (5)$$

$$F(i\omega_n)=-\frac{1}{N}\sum_j \int_0^\beta d\tau \exp(i\omega_n\tau)\langle \mathrm{T}_\tau \hat{c}_{j\uparrow}(\tau)\hat{c}_{j\downarrow}(0)\rangle, \quad (6)$$

where T_τ denotes time ordering in τ. The definitions of $\Sigma(i\omega_n)$ and $\phi(i\omega_n)$ for each calculation are given in the appendix, Eqs. (A2)–(A16), and are represented in Fig. 2.

The phonon propagator $D(i\omega_\nu)$ is defined by[26]

$$D(i\omega_\nu)=\frac{m\Omega^2}{N}\sum_j \int_0^\beta d\tau \exp[i\omega_\nu\tau]\langle T\hat{x}_j(\tau)\hat{x}_j(0)\rangle, \quad (7)$$

such that the bare propagator, with no self-energy, $D^{(0)}(i\omega_\nu)$, is equal to $-\Omega^2/(\omega_\nu^2+\Omega^2)$. The appropriate Matsubara frequencies ω_ν in this case, are those which lead to bosonic statistics, such that $i\omega_\nu=2\pi iT\nu$.

When we use bare phonons, and have no vertex corrections, the electron self-energy is illustrated in Fig. 2(a). The first term is the Hartree contribution Un. It can be included by a shift of the chemical potential as it only contributes a constant to the diagonal part of the self-energy $\Sigma(i\omega_n)$. Such a shift is implicitly included when μ appears in a Green's function, so that the Hartree term is hereafter neglected. It is followed by the Fock term, then a single-phonon dressing term, where the phonon line includes a single loop, which is the electron polarizability $\pi^{(0)}(i\omega_\nu)$:

$$\pi^{(0)}(i\omega_\nu)=-2T\sum_m [G(i\omega_m)G(i\omega_{m+\nu})$$
$$-F(i\omega_m)F^*(i\omega_{m+\nu})], \quad (8)$$

with the factor of 2 arising from the summation over spin. The third term includes dressing of phonons in a truncated manner, and allows us to make comparison with the complete second-order approximation, in Fig. 2(b), where the only difference is the inclusion of the vertex-correction term. The specific formula for the extra term in Fig. 2(b), which enters our calculations when we include vertex corrections using bare phonons, is given in Eqs. (A7) and (A8). The extra contributions to the self-energy coming from vertex corrections have opposite sign to the Fock term, near half filling, where the product of two electronic Green's functions is negative (the Green's functions are pure imaginary at half filling). Away from half filling, the Green's functions gain real parts, which means that near the band edges the product of two Green's functions can be positive, and the vertex-correction terms then add to the Fock term.

In the calculations with dressed phonons, we have a Dyson's equation for the phonon propagator, as depicted in Fig. 3,

$$D(i\omega_\nu)=D^{(0)}(i\omega_\nu)+D^{(0)}(i\omega_\nu)\Pi(i\omega_\nu)D(i\omega_\nu), \quad (9)$$

where $\Pi(i\omega_\nu)$ is the phonon self-energy. Note that within the conserving approximations, we must determine the phonon self-energy by differentiating the free-energy functional:

$$\Pi(i\omega_\nu)=\frac{-2}{T}\frac{\delta\Phi}{\delta D(i\omega_\nu)}. \quad (10)$$

With no vertex corrections, the phonon self-energy is simply given by the electron polarization, as depicted in Fig. 3(a). That is,

$$\Pi(i\omega_\nu)=U\pi^{(0)}(i\omega_\nu). \quad (11)$$

In this case, we use the contributions to the electron self-energy that are shown in Fig. 2(c), whose explicit formula is given in Eq. (A11). Note that the term with the single polarization bubble is missing, as all orders of such ''necklace''

diagrams are included in the Fock term with the dressed phonon propagator. In fact, the approximation including dressed phonons without vertex corrections is equivalent to the shielded potential approximation, whereby the infinite series of ring diagrams without vertex corrections are included in the skeleton-diagram functional Φ'.

When we include vertex corrections, as well as dressed phonons, the phonon self-energy gains the extra term shown in Fig. 3(b). The full expression is given in the Appendix [Eq. (A16)]. Note that a fully dressed phonon propagator is included in the phonon self-energy. As shown in Fig. 2(d), the electron self-energy now has the expected extra term with a crossing of phonon lines. It is almost identical to the extra term in Fig. 2(b), except of course, now the phonons are dressed. Again, the details of the formula can be found in the Appendix.

Our calculations all involve iteration of the Green's functions and self-energies, until a self-consistent solution is reached. We begin with the noninteracting Green's functions (set the self-energies to zero), and use it to calculate an initial estimate of the self-energies, according to Eqs. (A2)–(A16). The new self-energies are used to calculate updated Green's functions, according to Eqs. (3) and (9). The procedure is iterated, so that at each step there is an updated self-energy, which includes a fraction of the previous self-energy, the exact fraction variable, dependent upon the progress of the iteration. We stop the process when the change in all the self-energies is less than one part in 10^{-10}, which is typically after tens, but sometimes after hundreds of iteration steps.

Superconductivity occurs below a critical temperature T_c, where the normal state becomes unstable to fluctuations in the pairing potential (the Cooper instability). The instability shows itself as a divergence in the pairing susceptibility $\chi_{m,n}$ which is given by

$$\chi_{m,n}=\chi_m^{(0)}\delta_{m,n}-T\sum_l \chi_m^{(0)}\Gamma_{m,l}\chi_{l,m}, \tag{12}$$

where $\Gamma_{m,n}$ is the irreducible vertex function, to be defined shortly. The bare susceptibility in the superconducting channel for momentum $\mathbf{q}$ is defined as

$$\chi_m^{(0)}(\mathbf{q})\equiv\frac{1}{N}\sum_{\mathbf{k}} G(i\omega_m,\mathbf{k})G(-i\omega_m,-\mathbf{k}+\mathbf{q}), \tag{13}$$

which becomes in the local approximation (for the zero-momentum pair):

$$\chi_m^{(0)}=\frac{\mathrm{Im}[G(i\omega_m)]}{\omega_m Z(i\omega_m)}, \tag{14}$$

where

$$\omega_m Z(i\omega_m)=\omega_m-\mathrm{Im}[\Sigma(i\omega_m)]. \tag{15}$$

The transition temperature T_c occurs when the largest eigenvalue of the matrix $-T\chi_m^{(0)}\Gamma_{m,l}$ passes through unity. We calculate the highest eigenvalue using the power method.

The irreducible vertex function $\Gamma_{m,n}$ is given by the functional derivative of the off-diagonal self-energy, with respect to the off-diagonal Green's function

$$T\Gamma_{n,m}=\delta\phi(i\omega_n)/\delta F(i\omega_m). \tag{16}$$

As the pairing fluctuations lead to an instability of the normal state, $\Gamma_{n,m}$ must be calculated in the normal state [i.e., in the limit $F(i\omega_n)\mapsto 0$].

Figure 5 shows the contributions to the irreducible vertex function for each of the four approximations. Each diagram is achieved by removal of one electron Green's function line, from a self-energy diagram in Fig. 2. The algebraic expressions for each of the four sets of diagrams are given in the Appendix. Note that because the calculations are carried out in the normal state, with $F\mapsto 0$, rings within the self-energy can not be broken, as the resulting ladder diagrams give zero contribution. [Compare Fig. 5(a) arising from Fig. 2(a)].

As we wish to uncover more than the phase diagram given by the different perturbation approximations, we move on to describe how we calculate other properties. In order to find the superconducting gap and thermodynamic quantities, calculations are required within the superconducting state, but a simple addition to the previous computations in the normal state allows us to calculate the isotope coefficient.

The isotope coefficient α describes how the critical temperature changes with the phonon mass M. It is defined as

$$\alpha=-\frac{d\ln T_c}{d\ln M}, \tag{17}$$

so that $T_c\propto M^{-\alpha}$. The weak-coupling limit of BCS theory, and Migdal-Eliashberg theory with no Coulomb repulsion, predict $\alpha=0.5$, which corresponds to $T_c\propto 1/\sqrt{M}$. The phonon frequency changes with mass, according to $\Omega\propto 1/\sqrt{M}$, so both the product $M\Omega^2$ and the interaction energy U remain constant. Hence we calculate the isotope coefficient simply by changing the phonon frequency by 1% (corresponding to a typical mass change of 2% between isotopes) and comparing the change in critical temperature. To be precise, we compute α by

$$\alpha=0.5\cdot\frac{T_c^{(\mathrm{new})}-T_c^{(\mathrm{old})}}{T_c^{(\mathrm{old})}}\cdot\frac{\Omega^{(\mathrm{old})}}{\Omega^{(\mathrm{new})}-\Omega^{(\mathrm{old})}}, \tag{18}$$

so the BCS result is achieved if $T_c\propto\Omega$.

According to standard methods,[27–29] the energy gap in the superconducting state Δ requires a self-consistent calculation within the superconducting state. Note, the order parameter on the imaginary axis is related to the off-diagonal self-energy through

$$\Delta(i\omega_n)=\phi(i\omega_n)/Z(i\omega_n), \tag{19}$$

where $Z(i\omega_n)$ is the mass-enhancement parameter, calculated from the electronic self-energy $\Sigma(i\omega_n)$ as given in Eq. (15). The gap itself is found from the order parameter on the real axis, at the point where $\mathrm{Re}[\Delta(\omega)]=\omega$. We carry out a Padé analytic continuation[30,31] to obtain the order parameter on the real axis, and hence the value of the gap.

The free energy can be found from the formula[32–34]

$$F=-2T\sum_n \left\{\frac{1}{2}\ln[-1/\det \underline{\underline{G}}(i\omega_n)] + \frac{1}{2}\mathrm{Tr}\underline{\underline{\Sigma}}(i\omega_n)\underline{\underline{G}}(i\omega_n)\right\} + \frac{T}{2}\sum_\nu \{\ln[-1/D(i\omega_\nu)] + \Pi(i\omega_\nu)D(i\omega_\nu)\}+\Phi+\mu(n-1). \quad (20)$$

The free-energy functional Φ whose partial differential with respect to the electron (or phonon) Green's function gives the electron (or phonon) self-energy is depicted in Fig. 4 and evaluated in Eqs. (A2), (A6), (A11), and (A15). We are interested in the free-energy difference between normal and superconducting states at fixed electron filling n in which case the first, Hartree, term in Φ is neglected as it is a constant $Un^2/2$. The final term, $\mu(n-1)$ cannot be neglected, because the chemical potential can differ considerably between the superconducting and normal state when one includes the effects of nonconstant density of states.

We calculate the thermodynamic critical field in the superconducting state H_c from the free-energy difference between the superconducting and normal state, according to the formula $F_S-F_N=-\mu_0 H_c^2$. The thermodynamic field varies with temperature in an almost quadratic manner, so that calculation of the deviation function, which is defined as the difference between $H_c(T)$ and the quadratic form $H_c(0)[1-(T/T_c)^2]$ gives a sensitive test of changes in thermodynamic quantities.

In the calculations which include a Coulomb repulsion term U_C, we make the standard simplification[16,27–29] of only including its effects on the off-diagonal self-energy. This simplification is valid, as the normal-state Green's functions in reality include the Coulomb repulsion effects, and these change by very little for the diagonal part of the Green's function when superconducting order is present. As our model does not include the effects of U_C on the diagonal Green's functions, it is not strictly the solution of a simple Hamiltonian with a U_C term included.[35] However, the simplification does allow us to compare the effects of including a Coulomb repulsion versus adding vertex corrections, on the superconducting properties and transition temperature from a similar normal state and it is precisely the method employed in analyzing experimental data on real materials. With these comments understood, the only changes to the calculations that are necessary with the inclusion of a Coulomb term, are that both the off-diagonal self-energy $\phi(i\omega_n)$ and the irreducible vertex function $\Gamma_{n,m}$ gain an extra term:

$$\phi(i\omega_n)\mapsto\phi(i\omega_n)+U_C T\sum_m F(i\omega_m), \quad (21)$$

$$\Gamma_{n,m}\mapsto\Gamma_{n,m}+U_C. \quad (22)$$

In the computational calculations, the Matsubara frequency sum is cut off after a constant number N_c of terms. This leads to a renormalization which reduces the Coulomb term[16,36] to a pseudopotential U_C^* given by

$$U_C^*=U_C \Big/ \left\{1-2TU_C\sum_{N_c+1}^{\infty}\frac{\mathrm{Im}[G(i\omega_m)]}{\omega_m}\right\}, \quad (23)$$

where the diagonal Green's function $G(i\omega_m)$ is at high frequency, where the self-energies may be neglected, but must include the self-consistent chemical potential μ. In our calculations, with the frequency cutoff on the scale of the bandwidth such that 256 or 512 Matsubara frequencies are used, there is a very small (typically 1 or 2 %) reduction in U_C. This is different from the conventional approach in real materials because here our energy cutoff is governed by the electronic bandwidth, not some multiple of the maximum phonon frequency. To make contact with the standard formalism, we define a dimensionless pseudopotential $\mu_C^*=\rho^{(0)}(\mu)\cdot U_C^*$, where $\rho^{(0)}(\mu)$ is the noninteracting electronic density of states at the chemical potential. In calculations at different temperatures, U_C is kept fixed, so that μ_C^* varies to a small extent.

Finally, we wish to make clear how λ, the measure of the electron-phonon coupling strength, is defined in our work. A precise definition is required, because different methods of calculating λ lead to different results away from the weak-coupling limit, especially when the phonons are dressed. Here, λ is given by

$$\lambda=\rho^{(0)}(\mu)\cdot U\cdot D(0), \quad (24)$$

where $D(0)$ is the zero-frequency component of the *dressed* phonon propagator, which can be significantly different from that of the bare propagator $D^{(0)}(0)$. This value of λ is usually different from the electronic mass enhancement parameter, i.e., $\lambda\neq Z(0)-1$, as the two are only equal in the weak-coupling limit and with $\Omega\mapsto 0$. The definition of λ is identical to that commonly calculated from the electron-phonon spectral density,[27] $\alpha^2F(\omega)$, namely,

$$\lambda=2\int_0^\infty\frac{\alpha^2F(\omega)d\omega}{\omega}, \quad (25)$$

where

$$\alpha^2F(\omega)=\rho^{(0)}(\mu)|U|\frac{1}{\pi}\mathrm{Im}[D(\omega)]. \quad (26)$$

The real-axis form of the phonon propagator $D(\omega)$ is calculated from its imaginary-axis values $D(i\omega_\nu)$ by a Padé analytic continuation.

III. RESULTS

In choosing the parameters used to carry out the calculations, a number of criterion had to be satisfied. First, we wished to operate outside the weak-coupling regime, so that vertex corrections would not be negligible. The phonon frequency needed to be large compared to conventional low-temperature superconductors, but not so large that it gave no realistic point of contact with those superconductors mentioned in the introduction. So we choose $\Omega=t$, equal to one twelfth of the bandwidth. We had to ensure the electron-phonon coupling strength was not so strong that the ground state would contain bipolarons,[37] making the perturbation expansion about a Fermi liquid state invalid. A maximum cou-

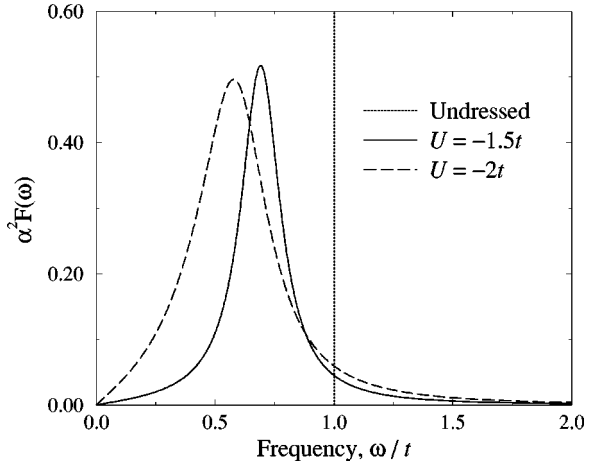

FIG. 6. $\alpha^2 F(\omega)$, calculated from the dressed phonon propagator on the real frequency axis for $n=1$ and $\Omega=t$. Increased coupling leads to a greater downwards shift in frequency from the initial delta function at $\omega=t$.

pling of $U=-2t$, hence a bare $\lambda<0.5$ ensured this. Finally, in order to calculate properties in an achievable time, while ensuring the imaginary frequency cutoffs were at energies larger than the band-width, the temperature of the calculations could not be too small, hence $T>2\times10^{-3}t$. The last condition meant that results within the superconducting state were best carried out for as large U and Ω as possible, so that T_c would be high. Hence, calculations near the band edges, where the density of states was low, prove to be inaccurate, due to the very low transition temperatures there.

Our first result is that dressing the bare phonon propagator leads to considerable renormalization effects. To be specific, the value of λ doubles from its bare value of $\lambda=0.21$, to $\lambda\approx0.4$ after dressing the phonons, using parameters $\Omega=t$ and $U=-1.5t$, near half filling. Moreover, at the increased interaction strength of $U=-2t$, λ is enhanced by a factor of 3 from the value of $\lambda=0.28$ for undressed phonons to the dressed value of $\lambda\approx0.9$. Such an enhancement indicates that the perturbation expansion would be inaccurate at bare coupling strengths lower than might be naively expected. Figure 6 shows how $\alpha^2F(\omega)$ is altered from its bare value, a delta function situated at $\omega=\Omega=t$, when it is dressed. Note that there is both a shift to lower frequencies as well as a broadening of the spectrum. The shift to lower frequencies shows that a Holstein model with bare phonon frequencies of near 10% of the bandwidth can be required to lead to dressed phonon frequencies at approximately 5% of the bandwidth. Hence the exact phonon self-energy used is an important factor when modeling electron-phonon systems, near the crossover between the weak-coupling and strong-coupling regimes.

The preceding paragraph explains some of the dramatic differences between the critical temperature (T_c) values for the different approximations, shown in Fig. 7. In particular, the T_c for dressed phonons is markedly higher than that for bare phonons, which is to be expected as λ is also higher. Note that the transition temperatures fall rapidly with increasing filling, above a filling of about $n=1.5$, as the electronic density of states drops significantly in this region. Vertex corrections seriously reduce T_c near half filling ($n=1$).

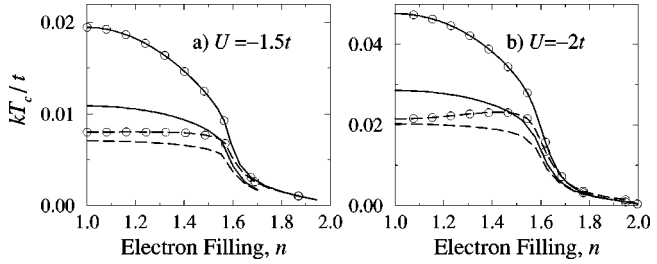

FIG. 7. Transition temperature as a function of filling. The dashed lines indicate vertex corrections are included, while solid lines are without them. The lines with circles have dressed phonons. Both diagrams show an enhanced T_c by dressing the phonons, while vertex corrections reduce T_c near half filling. In all cases, T_c falls rapidly above a filling of $n=1.55$, where the density of states drops rapidly.

The two curves with dressed phonons in Fig. 7 show a greater disparity than the two curves with bare phonons in the same figure, which means that dressing the phonons, which increases the effective coupling, enhances the effect of vertex corrections. Although it is hard to distinguish the curves due to the low T_c near the band edge, above a filling of $n=1.75$ the vertex corrections do lead to an enhancement of T_c. This result is in agreement with previous work.[12,14] Note that all results show particle-hole symmetry, that is, they are symmetric about half-filling. The figures just show half of the band ($n>1$), neglecting a mirror image below half filling.

It is clear that vertex corrections do change T_c by a considerable amount, but for any experimental measurement, where the microscopic parameters are not known, a Coulomb pseudopotential μ_C^* can always be fitted to give the same T_c as vertex corrections. Hence we continue with other results, to see where vertex corrections can not simply be mimicked by an appropriate μ_C^*, which would cause the effects of vertex corrections to be unobservable. So we fit a μ_C^* to give the same value of T_c as vertex corrections, and go on to change the unobservable electron-phonon coupling strength U to give the same λ as vertex corrections, when phonons are dressed. Hence the effects of vertex corrections can show up as discrepancies over a range of quantities compared to the values obtained with a fitted μ_C^* and λ.

Figure 8 is a direct comparison between the effects of vertex corrections and a Coulomb pseudopotential μ_C^* on the value of the gap parameter. Our first method is to fix the bare electron-phonon coupling and to adjust the value of U_C and hence μ_C^* in a calculation without vertex corrections, until the same T_c is reached as found in the calculation with vertex corrections [shown in Fig. 7(b)]. U_C is then used unchanged, to calculate other properties such as the gap parameter. The Coulomb pseudopotential μ_C^* varies with electron filling at T_c as shown in the inset. Notice that an artificial value of $\mu_C^*<0$ is required when $n>1.7$, as vertex corrections enhance T_c in this region. Near half filling, where μ_C^* is positive, and reduces T_c as vertex corrections, the gap parameter is reduced by a smaller amount. Hence a Coulomb repulsion leads to slightly higher gap ratio than vertex corrections.

The second curve, with a lower value of μ_C^*, is an alter-

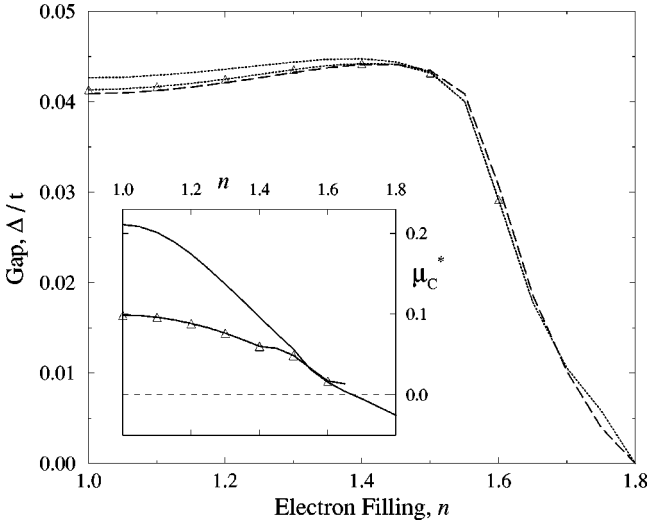

FIG. 8. A comparison between the effects of vertex corrections and a Coulomb pseudopotential, μ_C^* on the superconducting gap. The calculations are with dressed phonons, with $U=-2t$ and $\Omega=t$. The dashed curve is with vertex corrections, while the dotted curves include a μ_C^*, whose value changes with filling as shown in the inset, to ensure the two corresponding T_c curves are exactly the same. The dotted curve with triangles indicates a fit to the same λ by adjusting U as well as μ_C^*.

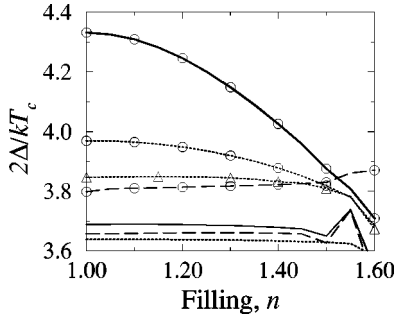

FIG. 9. Gap ratio $2\Delta/kT_c$ as a function of filling n. Dressed phonons (with circles) exhibit strong coupling behavior, by the increased gap ratio. Vertex corrections (dashed lines) reduce the effective coupling strength in the center of the band, hence the gap ratio is lower in this region. The dotted lines indicate how a Coulomb pseudopotential alters the gap ratio (when T_c is matched to T_c with vertex corrections, and where triangles indicate that λ is also matched, by adjusting U). With dressed phonons, the Coulomb repulsion clearly has less of an effect than do vertex corrections, but this is not the case with bare phonons.

nate approach, where both the dressed value of λ and T_c are fitted to the results with vertex corrections. A simple fit to T_c with a fixed bare coupling leads to a higher λ with a Coulomb repulsion than with vertex corrections, because λ is determined through the dressed phonon propagator. As a conventional analysis would fit λ to the experimental data, as well as μ_C^*, this second method follows the spirit of our paper by trying to fit conventional theory to the vertex-corrected results. In order to give the same values of λ, the electron-phonon interaction energy had to be varied, and in fact reduced by 10% at half filling. The result is a lower value of the gap ratio than with only μ_C^* fitted, but still a slightly larger value than with vertex corrections alone.

Although the magnitude of the gap varies considerably, depending upon the approximation used, Fig. 9 shows that the gap ratio $2\Delta/kT_c$ varies less markedly. The gap ratio is greater than 4 in the case of dressed phonons without vertex corrections, which is typical of the strong coupling regime ($\lambda>0.5$). Note that when the phonons are bare, so the coupling is less strong, the inclusion of vertex corrections, while strongly reducing T_c and Δ individually, has little effect on the ratio $2\Delta/kT_c$.

The isotope coefficient α has a value of 0.5 in the simplest, BCS, approximation, and in Migdal-Eliashberg theory with no Coulomb repulsion. The reason is that the phonon frequency provides the only cutoff for the coupling between different states, and phonon frequencies are proportional to $M^{-0.5}$, where M is the ionic mass. Inclusion of a frequency-independent Coulomb repulsion U_C leads to a reduction in α, as does a finite bandwidth. The reduction in α, indicates that the increase in phonon frequency is less effective at increasing T_c than otherwise. Higher-frequency phonons reduce the retardation in the electron-electron attraction, so the Coulomb repulsion between electrons is less shielded. The finite bandwidth means that the number of states coupled together includes a factor independent of phonon frequency, so T_c does not increase with Ω as it might if there were an infinite number of electron states extending through all energies.

It is known[38,16] that Migdal-Eliashberg theory with a finite bandwidth and including a Coulomb repulsion, leads to the allowed range of values for the isotope coefficient, $0\leqslant\alpha\leqslant0.5$. Including a nonconstant density of states[39,40] can in principle lead to any positive value of α. The reason being that T_c increases because extra electron states near the chemical potential are able to couple together when the phonon frequency increases. If the density of states increases significantly in the region of energy where new states are coupled together, the increase in T_c is much higher than would otherwise be expected, and α can be large, even greater than 0.5. The corollary is that if the density of states decreases away from the chemical potential, α also decreases, but never to less than zero, as T_c does not go down when the number of states coupled together goes up.

Figure 10 shows that the inclusion of vertex corrections in the calculations with dressed phonons not only reduces α, but can in fact lead to negative values. Indeed, the strongest reduction in α by vertex corrections occurs near half filling, and at strong coupling, where T_c is comparatively large. By comparison, in all cases the Coulomb pseudopotential, which gives the same reduction in T_c as vertex corrections, leads to a much smaller reduction in α. In Migdal-Eliashberg theory, a very small value of α requires a very low T_c.

Hence, any observation of isotope effects which have $\alpha<0$, or a small α with moderate to high T_c, implies that either vertex corrections are involved or some other mechanism outside of Migdal-Eliashberg theory is important. Paramagnetic impurities,[41,42] proximity effects,[43] anharmonicity,[44,45] and an isotopic dependence of the electron density in the conduction band,[42,43] can also lead to a low or negative α without requiring a low T_c. One or more of these effects may be important, in those materials with

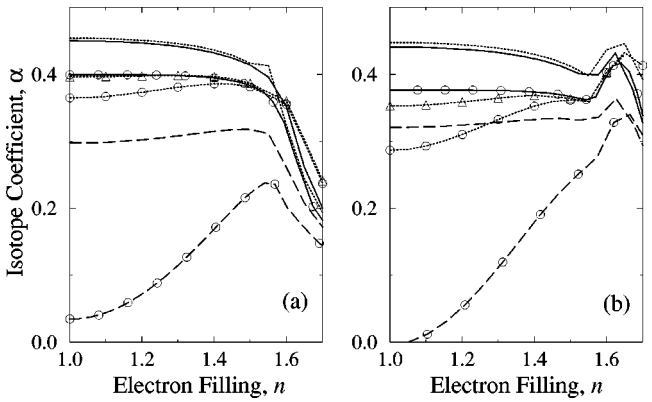

FIG. 10. The isotope coefficient α plotted against electron filling n for (a) $U=-1.5t$ and (b) $U=-2t$. Vertex corrections, indicated by dashed lines, reduce α. As does dressing the phonons, seen by the lines with circles. (b) exhibits the unusual feature of $\alpha<0$ for dressed phonons, with vertex corrections included. The dotted curve in (b) is the result with the Coulomb repulsion μ_C^* shown in the inset in the previous figure.

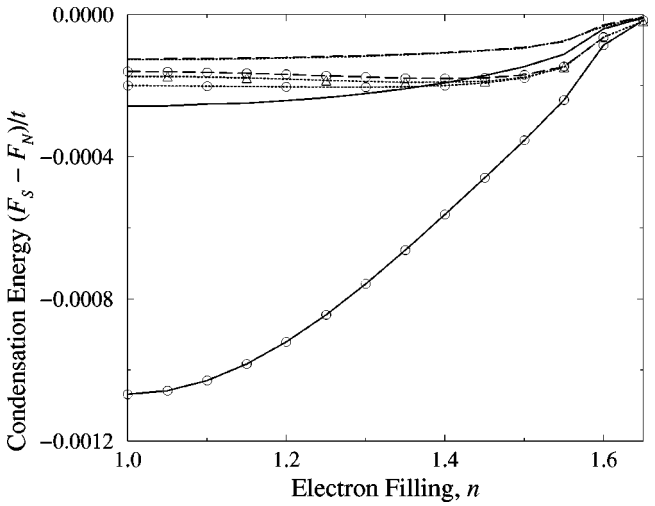

FIG. 11. Condensation energy, F_S-F_N. Circles indicate the phonons are dressed, which leads to a greater condensation energy. The dotted lines indicate dressed phonons with a Coulomb pseudopotential, to mimic the vertex-corrected T_c, the triangles indicating that U is also adjusted to mimic the λ obtained with vertex corrections. The dashed, vertex-corrected curve shows smaller condensation energy for $n<1.55$, though the difference can not be seen with bare phonons.

anomalously low values of α,[46–53] but vertex corrections should also be considered.

An important effect of dressing the phonons is that a small increase in the bare phonon frequency does not just result in a constant shift of $\alpha^2F(\omega)$, through a rescaling of the frequency variable. When calculating the isotope effect, it is common to assume that a mass substitution simply rescales the frequency, otherwise maintaining the same form of $\alpha^2F(\omega)$. However, the phonon self-energy is not independent of frequency, so the magnitude of $\alpha^2F(\omega)$ at its peak, which is inversely proportional to the imaginary part of the self-energy at that frequency, does not remain constant. In fact, the peak height is reduced by an increase in peak frequency, resulting in a slight reduction in λ. Hence the increase in T_c with bare frequency is less than otherwise expected, reducing the isotope coefficient for dressed phonons.

Interestingly, when the phonons are undressed, the Coulomb repulsion leads to a very small increase in α. This arises, because the term with a single polarization bubble (the first order term coming from dressed phonons) is present. The term acts to reduce α, but is less significant at the lower transition temperatures caused by the Coulomb pseudopotential. Meanwhile, the increase in μ^* with temperature, which acts to reduce α is a much smaller effect.

The free-energy difference $\Delta F=F_S-F_N$ is plotted as a function of filling n in Fig. 11. In the simplest picture, true in the weak-coupling limit, one expects the magnitude of the free-energy difference to be approximately equal to $\rho(\mu)\Delta^2/2$, representing a number of states $\rho(\mu)\Delta$ each shifted by an average energy of order $\Delta/2$. Although, with $\rho(\mu)$ given by $Z(0)\rho^{(0)}(\mu)$, the weak-coupling result predicts too high a condensation energy,[28] it does explain the qualitative changes between the different curves of Fig. 11.

In fact, the dimensionless quantity $\gamma T_c^2/(8\pi\Delta F)$ [the Sommerfeld constant, $\gamma=2\pi^2k_B^2\rho^{(0)}(\mu)Z(0)/3$] changes little for these curves. At half filling, with dressed phonons, the value is reduced from the BCS constant result of 0.168 to a strong-coupling value of 0.137. The value with vertex corrections is 0.157, while with the Coulomb pseudopotential it is 0.149. Hence, as with the gap ratio, near half filling, vertex corrections cause quantities to be closer to the weak-coupling values than does a Coulomb pseudopotential fitted for the same T_c. The values at a filling of $n=1.6$ are all closer to the weak-coupling limit, as expected when the density of states falls. The result is 0.163 for dressed phonons without vertex corrections, changing little to 0.165 with a Coulomb pseudopotential and 0.158 with vertex corrections.

It is worthwhile pointing out that the difference in thermodynamic potentials, which is usually calculated as an approximation to the free-energy difference, leads to very different results away from half filling. The approximation is based on the assumption that the chemical potential changes little between normal and superconducting states, but this is not necessarily the case when there is a nonconstant density of states. In fact, there is a particularly large shift from the normal-state chemical potential μ_N to that in the superconducting state μ_S if μ_N lies near the van Hove singularity, where the noninteracting density of states is falling precipitously. This can be understood, by considering how states above and below the normal-state chemical potential μ_N couple together and create an energy gap. When the density of states is falling rapidly with increasing energy, electronic states from a larger energy region above μ_N couple to those in a small region below μ_N. The resulting energy gap is skewed up in energy, so the chemical potential in the superconducting state μ_S, which sits in the middle of the gap, becomes greater than μ_N. In the mirrored example below half filling, near $n=0.4$, μ_S is also pushed away from half filling, so we find $\mu_S<\mu_N$ there.

The thermodynamic critical field H_c is effectively the square root of the free-energy difference, so shows qualitatively the same effects. H_c is known[27] to vary with temperature in a manner close to the behavior $H_c(T)=H_c(0)[1-(T/T_c)^2]$ which corresponds to the two-fluid model. The deviation function, plotted in Fig. 12, is the difference be-

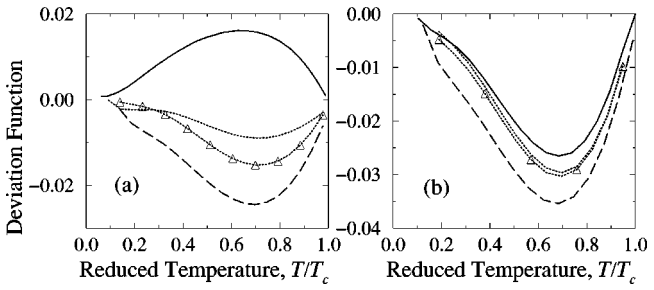

FIG. 12. Critical-field deviation function $H_c(T)/H_c(0)-[1-(T/T_c)^2]$. Solid lines are without, dashed lines are with vertex corrections. The dotted lines with and without triangles include the Coulomb pseudopotentials μ_C^* of Fig. 8, inset. All results are for dressed phonons. (a) is at half filling, $n=1$ while (b) is at a filling of $n=1.6$. Note the shift in scale for the second graph.

tween the reduced critical field $H_c(T)/H_c(0)$ and the quadratic fit $1-(T/T_c)^2$.

The curve without vertex corrections at half filling shows a small positive deviation, with a maximum of 0.02, typical of strong-coupling superconductors. Interestingly, when vertex corrections are included, the deviation function at half filling becomes negative, showing a minimum of about -0.03, which is more typical of weak-coupling superconductors (BCS theory predicts a minimum of -0.037). This result fits in with those for other properties, demonstrating that vertex corrections reduce the effective coupling strength, near half filling. A Coulomb pseudopotential, with the same power to reduce T_c as vertex corrections, also decreases the deviation function, but to a lesser extent than vertex corrections do so. This is still true when the value of λ is also fitted, by altering U as necessary. The calculations away from the band center, at $n=1.6$, lead to a negative deviation for all approximations. The reduced density of states at this filling leads to weak-coupling behavior.

Other thermodynamic quantities, which can be derived from the free-energy data, are affected in similar ways. That is, vertex corrections reduce the effective coupling strength, to a greater extent than does a Coulomb repulsion giving the same T_c. For example, vertex corrections reduce the specific heat jump, ΔC at T_c, as does a Coulomb repulsion to a lesser extent. The following results are obtained by a numerical differentiation, so are not completely accurate in themselves, (perhaps only to 10%) but as much of the error is systematic, the trends are reliable. At half-filling, the dimensionless quantity, $\Delta C/\gamma T_c$ is reduced from the strong-coupling value of 2.44, to 1.63 with vertex corrections and 1.88 with a Coulomb pseudopotential (the BCS result is 1.43). Again, notice the typical result that near half filling, vertex corrections lead to a weaker-coupling result than does inclusion of a Coulomb pseudopotential. At an electron filling of $n=1.6$, the results indicate less strong coupling, giving $\Delta C/\gamma T_c=1.66$ for dressed phonons, with the value reduced to 1.53 by vertex corrections, and to 1.44 by a Coulomb repulsion.

IV. CONCLUSIONS

We have completed a numerical investigation of the effects of vertex corrections, dressing phonons and a nonconstant density of states on the physical properties of strong-coupling superconductors. We solved the Holstein model, using four distinct perturbation theories, within conserving approximations.

The necessity of incorporating a realistic phonon self-energy is of considerable importance to those working with model Hamiltonians. The use of dressed phonons in the Holstein model, leads to a large renormalization of the parameters — in particular, the value of λ can be enhanced by a factor of 3, when its bare value of 0.28 would suggest the system is in the weak-coupling regime. Such an enhancement of λ reveals itself in increased T_c, α, Δ, H_c, and a gap ratio $(2\Delta/kT_c)$ greater than 4. The real-frequency data shows that the Einstein spectrum (a delta function at Ω) is both broadened and peaked at a lower frequency, when the bare, Einstein phonons are dressed.

The nonconstant density of states affects Migdal-Eliashberg results in both expected and unexpected ways. Firstly, all quantities which depend on the density of states as a parameter within Migdal-Eliashberg theory change in the expected manner as the electron band filling changes. Note that any sharp features in the normal electronic density of states have their effects reduced by the ''averaging'' over a large phonon frequency range. Hence the strong fall in T_c and Δ is expected at both small and large fillings ($n<0.45$ and $n>1.55$) due to the rapid fall in the density of states in our model. More subtle, is the result that the chemical potential shifts by a considerable amount between the normal and superconducting states, if it lies near a van Hove singularity. To observe such an effect, the superconductor would have to be coupled to one with a more constant density of states.

We find, in agreement with previous work,[11,12,14,15] that vertex corrections lead to results that correspond to a reduced effective strength of the electron-phonon coupling near half filling, but an increased coupling strength near the band edges. These effects are exemplified by reductions in critical temperature T_c, superconducting gap Δ, isotope coefficient α, and thermodynamic critical field H_c near half filling. As nearly all of these effects can be modeled by an appropriate Coulomb pseudopotential μ_C^* it makes it extremely difficult for any single experiment to reveal that vertex corrections have played a significant role. However, we do find some trends worth pointing out.

First, if there is difficulty in fitting both T_c and Δ with a given $\alpha^2F(\omega)$ and μ_C^*, then this is an indication that vertex corrections may contribute, since they affect the ratio $2\Delta/kT_c$ for fixed T_c, reducing it near half filling. Second, if the experimentally measured deviation function for the thermodynamic critical field lies below the predicted value [with a given $\alpha^2F(\omega)$ and μ_C^*] vertex corrections could be import ant. Thirdly, a theoretical prediction, ignoring vertex corrections, will overestimate the specific heat jump at T_c. Finally, a more striking result, is in the isotope coefficient α, which vertex corrections reduce much more markedly than does μ_C^*. Indeed, vertex corrections can lead to $\alpha<0$, which μ_C^* alone can never do.[16] Hence materials that have moderate to large T_cs, but small isotope coefficients can still be electron-phonon mediated superconductors with vertex corrections included. As the isotope coefficient is the single experimental

quantity affected the most by vertex corrections, it is important to consider materials which have α unexplained by Migdal-Eliashberg theory.

Anomalously low, and even negative isotope coefficients have been observed in materials, such as Ru,[46] α-uranium,[47] PdH,[48] and $La_{2-x}Sr_xCuO_4$,[49–51] where vertex corrections are probably not important, and other mechanisms, such as anharmonicity, conduction electron density variations and paramagnetic impurities play a role. However, a system such as Rb_3C_{60},[52,53] where the phonon frequency is a sizable fraction of the electron bandwidth, is much more likely to have vertex corrections affect the value of α.

Still, the best way to see the effects of vertex corrections is to directly view their contribution in the multiphonon region of a tunnel junction, or in the high-energy region of the optical conductivity. So, in order to unequivocally demonstrate the presence of strong vertex corrections in a material, more accurate dynamical measurements at energies beyond the highest phonon frequencies need to be carried out.

V. ACKNOWLEDGEMENTS

J.K.F. and P.M. would like to thank the Office of Naval Research for support under Grant No. N000149610828. E.J.N. thanks the Cottrell Scholar Program of Research Corporation for financial support and was also supported by the Natural Sciences and Engineering Research Council of Canada. We are grateful for useful discussions with J. W. Serene.

APPENDIX: CONSERVING APPROXIMATION FORMULA

In this appendix, we give the specific formulas for the free-energy functional, self-energy and irreducible vertex functions for each of the four conserving approximations. Figures 4, 5 are the representations of these equations as Feynman diagrams. Hereafter, we employ the shortened notation $G_n \equiv G(i\omega_n)$, $G_n^* \equiv G(-i\omega_n)$ and similarly for F_n, D_ν, and $\pi_\nu^{(0)}$. Note that the difference of two fermionic frequencies leads to a bosonic frequency, i.e., $D_{m-n} = D(i\omega_m - i\omega_n) = D(i\omega_\nu)$, where $\nu = m-n$.

The calculations with no vertex corrections and a bare phonon propagator have the free-energy functional

$$\Phi^{\text{bare}} = \frac{-UT^2}{2}\sum_{n,m} \text{Tr}[\underline{\underline{\tau}}_3 \underline{\underline{G}}_n]\,\text{Tr}[\underline{\underline{\tau}}_3 \underline{\underline{G}}_m] D^{(0)}(\omega = 0) + \frac{UT^2}{2}\sum_{n,m} \text{Tr}[\underline{\underline{\tau}}_3 \underline{\underline{G}}_n \underline{\underline{\tau}}_3 \underline{\underline{G}}_m] D^{(0)}_{n-m} + \frac{U^2T}{4}\sum_{\nu} [\pi^{(0)}_\nu D^{(0)}_\nu]^2, \tag{A1}$$

where $\pi_\nu^{(0)}$ is the electron polarizability, defined in Eq. (8). The inclusion of the $\underline{\underline{\tau}}_3$ matrices, ensures that each pair of off-diagonal Green's functions $F_n^* F_m$ corresponding to Cooper pair creation then annihilation, enters the product with a minus sign.

Functional differentiation with respect to the diagonal electron Green's function G_n and off-diagonal Green's function F_n^* leads respectively to the diagonal term in the self-energy $\Sigma(i\omega_n)$,

$$\Sigma^{\text{bare}}(i\omega_n) = UTn + UT\sum_m G_m D^{(0)}_{n-m} - U^2T\sum_m G_m \pi^{(0)}_{n-m}[D^{(0)}_{n-m}]^2, \tag{A2}$$

and the off-diagonal term $\phi(i\omega_n)$,

$$\phi^{\text{bare}}(i\omega_n) = -UT\sum_m F_m D^{(0)}_{n-m} - U^2T\sum_m F_m \pi^{(0)}_{n-m}[D^{(0)}_{n-m}]^2. \tag{A3}$$

We only require the superconducting vertex part, which is given by the derivative:

$$T\Gamma^{\text{bare}}_{n,m} = \delta\phi(i\omega_n)/\delta F_m, \tag{A4}$$

taken in the limit $F_m \mapsto 0$. Hence with bare phonons and no vertex corrections, the vertex function is that shown in Fig. 5(a):

$$\Gamma^{\text{bare}}_{n,m} = -UD^{(0)}_{n-m} - U^2\pi^{(0)}_{n-m}[D^{(0)}_{n-m}]^2. \tag{A5}$$

There is only one extra term which comes from the inclusion of vertex corrections in the free-energy functional. It is the diagram in Fig. 4(b) with crossed phonon lines, and is equal to

$$\Phi^{vc} = \frac{U^2T^3}{4}\sum_{n,m,l} \text{Tr}[\underline{\underline{\tau}}_3 \underline{\underline{G}}_n \underline{\underline{\tau}}_3 \underline{\underline{G}}_m \underline{\underline{\tau}}_3 \underline{\underline{G}}_l \underline{\underline{\tau}}_3 \underline{\underline{G}}_{n-m+l}] \times D^{(0)}_{n-m} D^{(0)}_{l-m}. \tag{A6}$$

The total free-energy functional for bare phonons with vertex corrections included is $\Phi^{\text{bare}} + \Phi^{vc}$.

The extra term in the self-energy is found by differentiation of the above term. For the diagonal and off-diagonal parts, respectively, this leads to

$$\Sigma^{vc}(i\omega_n) = U^2T^2\sum_{m,l} \{G_m[G_l G_{n-m+l} - F_l F^*_{n-m+l} - F_{n-m+l}F^*_l] - G^*_l F_m F^*_{n-m+l}\} D^{(0)}_{n-m} D^{(0)}_{l-m}, \tag{A7}$$

$$\phi^{vc}(i\omega_n) = U^2T^2\sum_{m,l} \{F_m[F^*_l F_{n-m+l} - G_l G_{n-m+l} - G^*_{n-m+l} G^*_l] - F_l G_m G^*_{n-m+l}\} D^{(0)}_{n-m} D^{(0)}_{l-m}, \tag{A8}$$

The extra term leads to the new self-energy $\Sigma = \Sigma^{\text{bare}} + \Sigma^{vc}$ and $\phi = \phi^{\text{bare}} + \phi^{vc}$.

When the vertex correction term is added to the self-energy, three new terms appear in the irreducible vertex function, coming from each of three Green's functions that can be differentiated. The extra diagrams in Fig. 5(b) contribute a total of

$$\Gamma^{vc}_{m,n}=U^2T\sum_l \{[-G_lG_{n-m+l}-G^*_{n-m+l}G^*_l]D^{(0)}_{n-m}D^{(0)}_{l-m} - G_lG^*_{n+m-l}D^{(0)}_{n-l}D^{(0)}_{m-l}\}, \quad \text{(A9)}$$

leading to $\Gamma_{m,n}=\Gamma^{\rm bare}_{m,n}+\Gamma^{vc}_{m,n}$ as the irreducible vertex function for bare phonons, with vertex corrections.

The calculations with no vertex corrections, but a dressed phonon propagator have the free-energy functional

$$\Phi^{\rm dressed}=\frac{-UT^2}{2}\sum_{n,m} {\rm Tr}[\underline{\underline{\tau}}_3\underline{\underline{G}}_n]{\rm Tr}[\underline{\underline{\tau}}_3\underline{\underline{G}}_m]D^{(0)}(\omega=0) + \frac{UT^2}{2}\sum_{n,m} {\rm Tr}[\underline{\underline{G}}_n\underline{\underline{G}}_m]D_{n-m}. \quad \text{(A10)}$$

Functional differentiation with respect to the diagonal electron Green's function G_n and off-diagonal Green's function F^*_n leads respectively to the diagonal term in the electron self-energy $\Sigma^{\rm dressed}(i\omega_n)$,

$$\Sigma^{\rm dressed}(i\omega_n)=Un+UT\sum_m G_mD_{n-m} \quad \text{(A11)}$$

and the off-diagonal term $\phi^{\rm dressed}(i\omega_n)$,

$$\phi^{\rm dressed}(i\omega_n)=-UT\sum_m F_mD_{n-m}. \quad \text{(A12)}$$

Similarly, differentiation with respect to the dressed phonon propagator leads to the phonon self-energy

$$\Pi^{(1)}(i\omega_\nu)=-2UT\sum_m [G_mG_{m+\nu}-F_mF^*_{m+\nu}], \quad \text{(A13)}$$

where the factor of 2 indicates a sum over electron spins.

The superconducting vertex function still retains its simple form, differentiation of Eq. (A12) giving

$$\Gamma^{\rm dressed}_{n,m}=-UD_{n-m}. \quad \text{(A14)}$$

Analogously to the case of bare phonons, there is only one extra term which comes from vertex corrections in the free-energy functional. It is equal to

$$\Phi^{vc2}=\frac{U^2T^3}{4}\sum_{n,m,l} {\rm Tr}[\underline{\underline{\tau}}_3\underline{\underline{G}}_n\underline{\underline{\tau}}_3\underline{\underline{G}}_m\underline{\underline{\tau}}_3\underline{\underline{G}}_l\underline{\underline{\tau}}_3\underline{\underline{G}}_{n-m+l}] \times D_{n-m}D_{l-m}, \quad \text{(A15)}$$

where now the total free-energy functional for dressed phonons with vertex corrections included is $\Phi^{\rm dressed}+\Phi^{vc2}$.

Differentiation of the above contribution now leads to an extra term in the phonon self-energy Π^{vc}, as well as the extra electronic self-energy terms. Π^{vc} is the term shown with crossed phonon lines in Fig. 3(b):

$$\Pi^{vc}(i\omega_\nu)=-U^2T^2\sum_{m,l} {\rm Tr}[\underline{\underline{\tau}}_3\underline{\underline{G}}_{m+\nu}\underline{\underline{\tau}}_3\underline{\underline{G}}_m\underline{\underline{\tau}}_3\underline{\underline{G}}_l\underline{\underline{\tau}}_3\underline{\underline{G}}_{l+\nu}] \times D_{l-m}. \quad \text{(A16)}$$

Hence the full phonon self-energy is now $\Pi(i\omega_\nu)=\Pi^{(1)}(i\omega_\nu)+\Pi^{vc}(i\omega_\nu)$. The vertex functions and self-energies for electrons gain terms equivalent to those in Eqs. (A7)–(A9) only with bare phonon propagators $D^{(0)}_\nu$ replaced by dressed ones D_ν.

In the normal state, the expressions for the free-energy functionals and self-energies are simplified, by setting all off-diagonal contributions to zero, $F_n=0$ and $\phi(i\omega_n)=0$. Note that the above formulas for irreducible vertex functions are only calculated in the normal state.

To conclude, we present the explicit form for the skeleton-diagram expansion of the functional Φ' in terms of the free-energy functional Φ, which has been calculated above:

$$\Phi'=\frac{T}{2}\sum_\nu \{\ln[-1/D(i\omega_\nu)] - \ln[-1/D^{(0)}(i\omega_\nu)]+\Pi(i\omega_\nu)D(i\omega_\nu)\}+\Phi \quad \text{(A17)}$$

$$=\frac{T}{2}\sum_\nu \{\ln[1-D^{(0)}(i\omega_\nu)\Pi(i\omega_\nu)] + \Pi(i\omega_\nu)D(i\omega_\nu)\}+\Phi \quad \text{(A18)}$$

It can be noted that when the phonons are not dressed $[\Pi(i\omega_\nu)=0]$ then $\Phi'=\Phi$.

[1] J. Bardeen, L. N. Cooper, and J. R. Schrieffer, Phys. Rev. **108**, 1175 (1957).

[2] A. B. Migdal, Zh. Eskp. Teor. Fiz. **34**, 1438 (1958) [Sov. Phys. JETP **7**, 999 (1958)].

[3] G. M. Éliashberg, Zh. Eskp. Teor. Fiz. **38**, 966 (1960) [Sov. Phys. JETP **11**, 696 (1960)].

[4] L. F. Mattheiss, E. M. Gyorgy, and D. W. Johnson, Jr., Phys. Rev. B **37**, 3745 (1988).

[5] R. J. Cava, B. Batlogg, J. J. Krajewski, R. Farrow, L. W. Rupp, Jr., A. E. White, K. Short, W. F. Peck, and T. Kometani, Nature (London) **322**, 814 (1988).

[6] P. Vashishta, R. K. Kalia, M. H. Degani, D. L. Price, J. D. Jorgensen, D. G. Hinks, B. Dabrowski, A. W. Mitchell, D. R. Richards, and Y. Zheng, Phys. Rev. Lett. **62**, 2628 (1989).

[7] L. F. Mattheiss and D. R. Harman, Phys. Rev. Lett. **60**, 2681 (1988).

[8] A. F. Hebard, M. J. Rosseinsky, R. C. Haddon, D. W. Murphy, S. H. Glarum, T. T. M. Palstra, A. P. Ramirez, and A. R. Kortan, Nature (London) **350**, 600 (1991).

[9] K. Holczer, O. Klein, S.-M. Huang, R. B. Kaner, K.-J. Fu, R. L. Whetten, and F. Diederich, Science **252**, 1154 (1991).

[10] M. J. Rosseinsky, A. P. Ramirez, S. H. Glarum, D. W. Murphy, R. C. Haddon, A. F. Hebard, T. T. M. Palstra, A. R. Kortan, S. M. Zahurak, and A. V. Makhija, Phys. Rev. Lett. **66**, 2830 (1991).

[11] J. K. Freericks, Phys. Rev. B **50**, 403 (1995).

[12] J. K. Freericks, E. J. Nicol, A. Y. Liu, and A. A. Quong, Phys. Rev. B **55**, 11 651 (1997).

[13] J. K. Freericks and D. J. Scalapino, Phys. Rev. B **49**, 6368 (1993).
[14] E. J. Nicol and J. K. Freericks, Physica C **235-40**, 2379 (1994).
[15] J. K. Freericks and M. Jarrell, Phys. Rev. B **50**, 6939 (1994).
[16] F. Marsiglio, J. Low Temp. Phys. **87**, 659 (1992).
[17] T. Holstein, Ann. Phys. (N.Y.) **8**, 352 (1959).
[18] G. Baym and L. P. Kadanoff, Phys. Rev. **124**, 287 (1961).
[19] G. Baym, Phys. Rev. **127**, 1391 (1962).
[20] C. de Dominicis and P. C. Martin, J. Math. Phys. **5**, 14 (1964); **5**, 31 (1964).
[21] N. E. Bickers and D. J. Scalapino, Ann. Phys. (N.Y.) **193**, 206 (1989).
[22] J. K. Freericks, M. Jarrell, and D. J. Scalapino, Europhys. Lett. **25**, 37 (1994).
[23] C. S. Owen and D. J. Scalapino, Physica C **55**, 691 (1971).
[24] Y. Nambu, Phys. Rev. **117**, 648 (1960).
[25] G. S. Uhrig, Phys. Rev. B **54**, 10 436 (1996).
[26] A. L. Fetter and J. D. Walecka, *Quantum Theory of Many-Particle Systems* (McGraw-Hill, New York, 1971).
[27] J. P. Carbotte, Rev. Mod. Phys. **62**, 1027 (1990).
[28] D. J. Scalapino, in *Superconductivity*, edited by R. D. Parks (Marcel Dekker, New York, 1967).
[29] P. B. Allen and B. Mitrović, Solid State Phys. **37**, 1 (1982).
[30] H. J. Vidberg and J. W. Serene, J. Low Temp. Phys. **29**, 179 (1977)
[31] C. R. Leavens and D. S. Ritchie, Solid State Commun. **153**, 137 (1985).
[32] G. M. Éliashberg, Zh. Eskp. Teor. Fiz. **43**, 1005 (1962) [Sov. Phys. JETP **16**, 780 (1963)].
[33] J. Bardeen and M. Stephen, Phys. Rev. **136**, A1485 (1964).
[34] J. M. Luttinger and J. C. Ward, Phys. Rev. **118**, 1417 (1960).
[35] J. K. Freericks and M. Jarrell, Phys. Rev. Lett. **75**, 2570 (1995).
[36] N. N. Bogoliubov, N. V. Tolmachev, and D. V. Shirkov, *A New Method in the Theory of Superconductivity* (Consultants Bureau, New York, 1959).
[37] A. S. Alexandrov, Physica C **158**, 337 (1989).
[38] J. W. Garland, Jr., Phys. Rev. Lett. **11**, 114 (1963).
[39] E. Schachinger, M. G. Greeson, and J. P. Carbotte, Phys. Rev. B **42**, 406 (1990).
[40] J. P. Carbotte and E. J. Nicol, Physica C **185-9**, 162 (1991).
[41] J. P. Carbotte, M. Greeson and A. Perez-Gonzalez, Phys. Rev. Lett. **66**, 1789 (1991).
[42] A. Bill, V. Z. Kresin, and S. A. Wolf, Z. Phys. B **104**, 759 (1997).
[43] V. Z. Kresin, A. Bill, S. A. Wolf, and Yu. N. Ovchinnikov, Phys. Rev. B **56**, 107 (1997).
[44] S. L. Drechsler and N. M. Plakida, Phys. Status Solidi B **144**, K113 (1987).
[45] T. Galbaatar, S. L. Drechsler, N. M. Plakida, and G. M. Vujičić, Physica C **176**, 496 (1991).
[46] G. Gladstone, M. A. Jensen, and J. R. Schrieffer, in *Superconductivity* (Ref. 28).
[47] R. D. Fowler, J. D. G. Lindsay, R. W. White, H. H. Hill, and B. T. Matthias, Phys. Rev. Lett. **19**, 892 (1967).
[48] B. Stritzker and W. Buckel, Z. Phys. **257**, 1 (1972).
[49] J. P. Franck, S. Harker, and J. H. Brewer, Phys. Rev. Lett. **71**, 283 (1993).
[50] B. Batlogg, G. Kourouklis, W. Weber, R. J. Cava, A. Jayaraman, A. E. White, K. T. Short, L. W. Rupp, and E. A. Rietman, Phys. Rev. Lett. **59**, 912 (1987).
[51] T. A. Faltens, W. K. Ham, S. W. Keller, K. J. Leary, J. N. Michaels, A. M. Stacy, and H.-C. zur Loye, Phys. Rev. Lett. **59**, 915 (1987).
[52] A. P. Ramirez, A. R. Kortan, M. J. Rosseinsky, S. J. Duclos, A. M. Mujsce, R. C. Haddon, D. W. Murphy, A. V. Makhija, S. M. Zahurak, and K. B. Lyons, Phys. Rev. Lett. **68**, 1058 (1992).
[53] Yu. N. Garstein, A. A. Zakhidov, and E. M. Conwell, Phys. Rev. B **49**, 13 299 (1994).